Contributions to Mineralogy and Petrology (2020) 175:72
https://doi.org/10.1007/s00410-020-01708-x

ORIGINAL PAPER

Carbonate melts in the hydrous upper mantle

Daniel Weidendorfer[1,2] · Craig E. Manning[2] · Max W. Schmidt[3]

Received: 20 February 2020 / Accepted: 16 June 2020

Abstract
Carbonatite compositions resulting from melting of magnesian calcite + olivine + clinopyroxene were experimentally determined in the system CaO–MgO–SiO_2–CO_2–H_2O as a function of temperature and bulk H_2O contents at 1.0 and 1.5 GPa. The melting reaction and melt compositions were found to be highly sensitive to H-loss or -gain during experiments. We hence designed a new hydrogen-trap technique, which provided sufficient control to obtain consistent results. The nominally dry solidus temperatures at 1.0 and 1.5 GPa are 1225–1250 °C and 1275–1300 °C, respectively. At 1.0 GPa, the solidus temperature decreases with H_2O increasing to 3.5 wt% (1025–1050 °C), then remains approximately constant at higher H_2O concentrations. Our nominally dry solidus temperatures are up to 140 °C higher than in previous studies that did not take measures to limit hydrogen infiltration and hence suffered from H_2O formation in the capsule. The near-solidus anhydrous melts have 7–8 wt% SiO_2 and molar Ca/(Ca + Mg) of 0.78–0.82 (X_{Ca}). Melting temperatures decrease by as much as 200 °C with increasing X_{H_2O} in the coexisting COH-fluid. Concomitantly, near-solidus melt compositions change with increasing bulk H_2O from siliceous Ca-rich carbonate melts to Mg-rich silico-carbonatites with up to 27.8 wt% SiO_2 and 0.55 X_{Ca}. The continuous compositional array of Ca–Mg–Si carbonatites demonstrates the efficient suppression of liquid immiscibility in the alkali-free system. Diopside crystallization was found to be sensitive to temperature and bulk water contents, limiting metasomatic transformation of carbonated upper mantle to wehrlite at 1.0–1.5 GPa to < 1175 °C and < 7 wt% bulk H_2O.

Keywords Carbonatite · Mantle metasomatism · Wehrlite formation · Hydrogen diffusion

Introduction

Carbon is one of the most versatile elements with a remarkable chemical bonding flexibility and a range in oxidation numbers (− 4 to + 4) that enable its participation in chemical and physical exchange dynamics between the Earth's core, mantle, crust and atmosphere (Hazen et al. 2013; Wood et al. 2013). More than 500 occurrences of carbonate rocks of igneous origin (carbonatites) and large quantities of CO_2 being emitted along active volcanic systems to the atmosphere provide direct evidence for the importance of carbon in large-scale igneous processes in the deep Earth. Experimental studies on simplified carbonate–peridotite systems have proven essential to unravel the lithospheric carbon cycle (Dasgupta and Hirschmann 2010) and to understand the boundary conditions of carbonatite formation in the upper mantle (Wyllie and Huang 1976; Wallace and Green 1988; Falloon and Green 1989). Melting of carbonated peridotites (Olafsson and Eggler 1983; Wallace and Green 1988; Brey et al. 2009; Tumiati et al. 2013) and eclogites (Yaxley and Brey 2004; Dasgupta et al. 2004) is generally restricted to hot mantle regimes (> 1020 °C), although solidi in H_2O-rich subduction environments decrease to as little as 870–900 °C (Poli 2015). Disagreement persists on melting temperatures and melt compositions in anhydrous and H_2O-bearing carbonate model systems.

Communicated by Mark S Ghiorso.

Electronic supplementary material The online version of this article (https://doi.org/10.1007/s00410-020-01708-x) contains supplementary material, which is available to authorized users.

✉ Daniel Weidendorfer
d.weidendorfer@lmu.de

[1] Department of Earth and Environmental Sciences, LMU Munich, Theresienstrasse 41, 80333 Munich, Germany

[2] Department of Earth, Planetary, and Space Sciences, University of California Los Angeles, 595 Charles Young Drive East, Los Angeles, CA 90095-1567, USA

[3] Institute of Geochemistry and Petrology, ETH, Clausiusstrasse 25, 8092 Zurich, Switzerland

Published online: 16 July 2020

Near-solidus carbonate melt compositions in the model system CaO–MgO–SiO_2–CO_2 range from 2 to 3 wt% SiO_2 at 1150 °C, 1.5 GPa (Dalton and Wood 1993), to ≥ 11 wt% SiO_2 at 1100 °C, 1.0 GPa (Lee and Wyllie 2000). Dalton and Wood (1993) added minor H_2O to their synthetic starting mixture; however, they did not quantify its concentration or its effect on the resulting carbonate melt composition. In contrast, Lee and Wyllie (2000) performed nominally anhydrous experiments using single-Pt capsules.

The major problem in this type of experiment is controlling hydrogen, which readily diffuses through any metal capsule wall in response to gradients in hydrogen activity (a_{H_2}) (Huebner 1971; Chou and Eugster 1978). Experimental charges may either gain hydrogen from the piston cylinder assembly during nominally dry experiments or from redox-sensitive H_2O dissociation at high temperatures in COH-bearing systems, the graphite furnace supplying any required carbon (Eugster 1957; Luth 1989). In Fe-free carbonate-bearing experimental charges, H infiltration leads to the reduction of CO_2 or carbonate ions to graphite and molecular H_2O. Previous studies in the carbonated lherzolite system at 1–3 GPa did not account for hydrogen gain or loss during high-temperature experiments (Dalton and Wood 1993; Lee et al. 2000; Lee and Wyllie 2000) and some of the reported phase equilibria on "dry" melting have likely been compromised by unconstrained quantities of newly formed H_2O.

Here we investigate nominally dry and H_2O-assisted melting of forsterite + carbonate, which may serve as a model carbonated peridotite in CaO–MgO–SiO_2–CO_2–H_2O at 1.0 and 1.5 GPa. We first document the effects of H-gain through noble metal capsule walls on phase equilibria and on carbonate melt compositions in initially dry, unbuffered experiments. We then show the differences when using an H-trap double-capsule technique that effectively prevents the experimental charge from gaining hydrogen. Our experiments confirm the profound impact of hydrogen on melting CO_2-bearing upper mantle and suggest that metasomatic transformation of carbonated lherzolite to wehrlite is restricted to a narrow temperature–bulk H_2O window.

Starting materials and methods

Starting compositions

Starting compositions are shown in Table 1. System A is a mixture of 80 or 40 wt% synthetic forsterite (Fo) with 20 or 60 wt% of either natural calcite (Cc) or two synthetic high-purity carbonates mixed in proportions such that $Ca_{0.95}Mg_{0.05}CO_3$ or $Ca_{0.7}Mg_{0.3}CO_3$ result. The Fe-bearing system B was made of either 90 wt% natural San Carlos olivine (Fo_{91}, Arizona, USA) and one of the above synthetic carbonate mixtures or consisted of 40 wt% San Carlos olivine + 60 Cc. For fluid-saturated experiments, H_2O was either added as $Mg(OH)_2$, in which case SiO_2 was added to form Fo + H_2O, or liquid H_2O was inserted into the capsule with a microliter syringe. The purity of synthetic Fo was checked by electron microprobe and by X-ray diffraction to make sure no other phase had formed during olivine synthesis at high temperature. All starting materials were finely ground in the absence of water or any OH-bearing solvents and were permanently stored at 110 °C to avoid hydration from air.

Experimental methods

Phase equilibrium in CaO–MgO–SiO_2–CO_2–H_2O was investigated using a piston cylinder apparatus at 1.0 and 1.5 GPa and 1025–1350 °C in 25–50 °C intervals. To minimize H-gain and to realize nearly anhydrous conditions, we employed a newly developed double-capsule H-trap technique (Fig. 1a). An inner capsule of $Au_{50}Pd_{50}$ (0.7 mm length, OD 2 mm) was loaded with the starting material, welded and placed into an outer 4–5 mm OD Pt capsule that was loaded prior welding with a mix of homogenized Fo–carbonate powder. The Fo–carbonate mix in the outer Pt capsule acts as a trap for infiltrating hydrogen by reducing part of the available CO_2 or CO_3^{2-} from the Fo–carbonate mix in the outer capsule to graphite according to

$$2H_2 + CO_2 = 2H_2O + C. \quad (1)$$

Table 1 Major oxide composition of starting mixes for static high-pressure / -temperature experiments

System	Mix in weight percent	SiO_2	MgO	CaO	FeO	CO_2
A1	80Fo + 20Cc	27.0	54.0	9.5	–	9.5
A2	80Fo + 20$Ca_{95}Mg_5CO_3$	27.0	54.5	9.0	–	9.6
A3	80Fo + 20$Ca_{70}Mg_{30}CO_3$	26.7	56.8	6.6	–	9.9
A4	40Fo + 60Cc	13.9	27.7	29.2	–	29.2
B1	90Fo[a] + 10$Ca_{95}Mg_5CO_3$	30.2	54.6	4.8	5.4	5.0
B2	90Fo[a] + 10$Ca_{70}Mg_{30}CO_3$	30.1	55.8	3.5	5.3	5.2
B3	40Fo[a] + 60Cc	16.3	19.7	33.6	3.5	26.9

[a]Natural San Carlos olivine with Fo_{91}

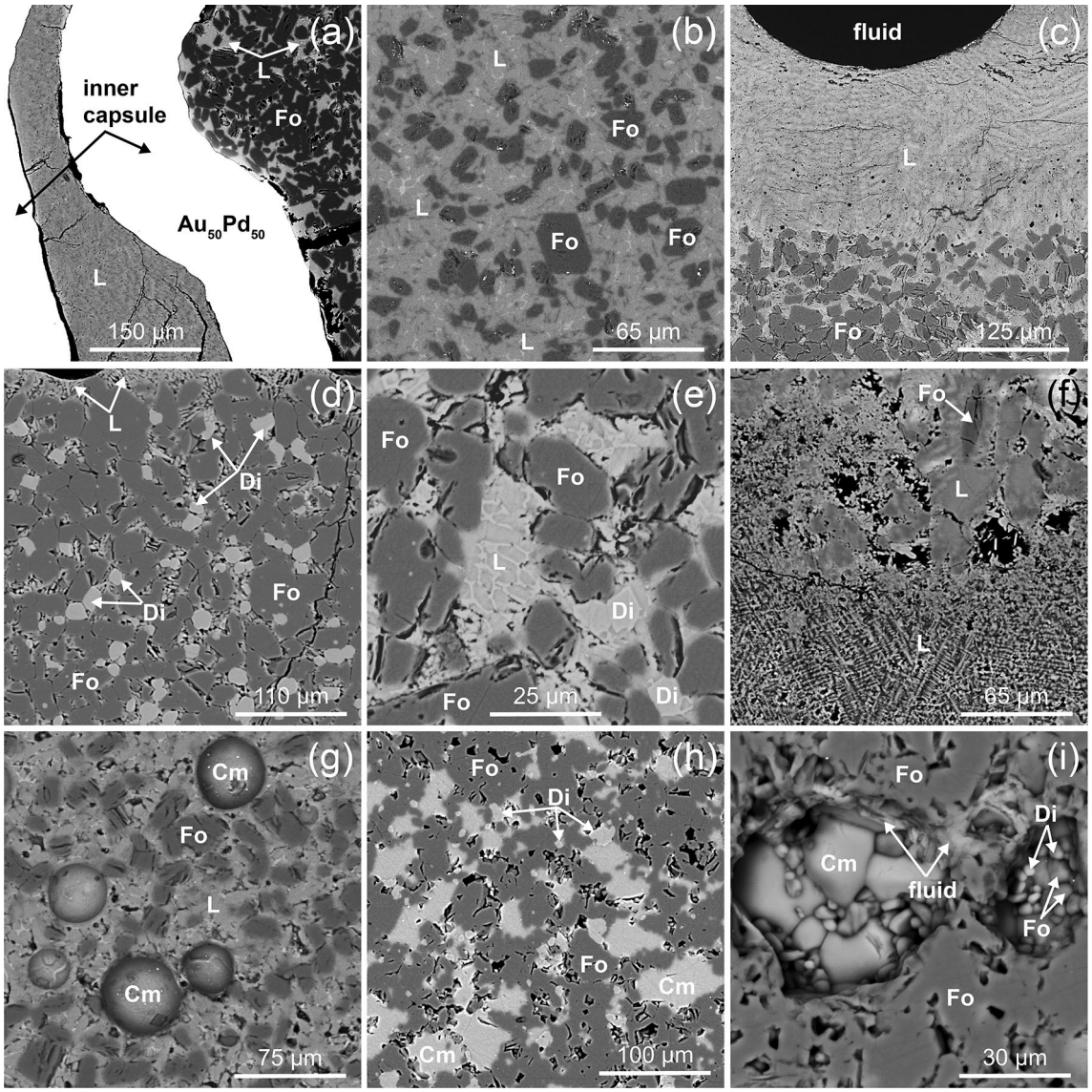

Fig. 1 Back-scattered electron images (BSE) of representative experimental charges. **a** H_2-trap double-capsule technique consisting of an inner $Au_{50}Pd_{50}$ capsule with the silicate + carbonate starting mix and an outer Pt-capsule with the forsterite + carbonate hydrogen-trap surrounding the inner $Au_{50}Pd_{50}$ target capsule. Essentially, any H diffusing from the piston cylinder assembly into the outer capsule reacts with the carbonate to form graphite + H_2O, the latter is dissolved in the consequently resulting (hydrous) carbonate melt. A schematic drawing of the double-capsule design is shown in the Supplementary Material S2. **b**, **c** Buffered anhydrous large carbonate weight fraction ($Fo_{60}Cc_{40}$) experiments show euhedral Fo embedded in carbonate liquid. Fo crystals in **c** settled at the bottom of the capsule with a large carbonate melt pool and void space at the top. **b** was run at 1275 °C, 1.0 GPa and **c** at 1300 °C, 1.5 GPa. **d** Metasomatic wehrlite forms in the hydrous melting regime at temperatures < 1175 °C. Unbuffered carbonate liquid in equilibrium with Fo + Di at 1150 °C, 1.5 GPa. **e**, **f** Quenched textures of carbonate liquids are characterized by CaMg dendritic intergrowth and a finely developed Si-rich honeycomb filaments. Carbonate melt in **f** quenched along the capsule wall to glass. **g** Large carbonate melt fraction experiment with the H_2-trap at 1200 °C, 1.0 GPa with 1 wt% bulk H_2O. Diopside is absent at temperatures exceeding 1175 °C. Metastable spherical calcite globules are present in a majority of our hydrous melting experiments at temperatures above the Mg-calcite-out phase boundary (Fig. 2). Metastable Mg-calcite-globules disappear after 22–25 h run time. **h**, **i** Subsolidus phase assemblage consists of Fo + Mg–calcite + Di in the nominally anhydrous and hydrous system. **i** In presence of a COH-fluid the inner surface of spherical fluid voids occasionally preserved quenched fluid deposits coexisting at subsolidus conditions with recrystallized Fo + Mg–calcite minute crystals. *Fo* forsterite, *Mg-calcite* magnesian calcite, *Di* diopside, *L* melt

H_2O from this redox reaction lowers the solidus of the remaining carbonate fraction (Wyllie and Tuttle 1960) initiating hydrous melting in the outer Pt-capsule. In our experiments, the carbonate melt in the outer capsule acts as a sink for H_2O due to its overall high H_2O solubility (~ 10 wt% at 0.1 GPa and 900 °C; Keppler 2003), which prevents the AuPd-encapsulated target sample from gaining additional

hydrogen on the time scales of our experiments (Fig. 1a). This buffer technique allows investigation of phase equilibria and melting relationships in the CaO–MgO–SiO_2–CO_2–H_2O model system under dry- and controlled hydrous conditions.

Experiments using the H-trap double-capsule technique were carried out in 2.54-cm-diameter end-loaded piston cylinders utilizing NaCl–Pyrex–graphite assemblages. Boron nitride and Pyrex surrounding the noble metal capsule were thought to limit H-gain during high-temperature experiments (Wendlandt et al. 1982). We, therefore, placed the double capsule with two boron nitride (BN) shoulder pieces horizontally into the hot spot of the graphite heater. Finely ground Pyrex filled the remaining space between the capsule and the BN shoulder pieces, subsequently sandwiched on top and bottom by BN discs. The graphite heater was then filled with upper and lower AlSiMg ceramic cylinders.

Pressure calibration was carried out for the NaCl–Pyrex-AlSiMg–BN assembly by determining the melting temperature of albite (Boyd and England 1963). No pressure correction was required for the pressure range of interest. The loaded assemblies were pressed cold to 3 kbar, then heated to 700 °C to ensure a plastic behavior of the Pyrex. Pressure was then increased to the desired value before the sample was heated to the temperature of interest. Pressure increased upon heating but was held at the desired value by bleeding hydraulic oil.

Experiments allowing for H-diffusion were carried out in single-welded Pt capsules embedded in NaCl–graphite–BN–MgO assemblies. Samples were pressed cold to 75% of the desired pressure and then heated. Pressure calibration is based on quartz solubility in H_2O (Manning 1994), a friction correction of − 0.6 kbar was required.

Temperature was measured by Pt–$Pt_{90}Rh_{10}$ (S-type) thermocouples in contact with a Pt thermocouple shield on top of the capsule. Experimental runs were 5–92 h in duration and terminated by cutting the heating power. Initial quench rates were > 200 °C/s. After each experiment, inner capsules were first cleaned of surrounding buffer material, weighed, then pierced with a stainless-steel needle and weighed again. The weighing checks for fluid leakage during the experiment and determine the weight change resulting from gas escape.

Analytical methods

Inner capsules were embedded in epoxy, polished with oil-based diamond solutions and carbon coated. The capsules are embedded such that the polished surface exposed a vertical cross section through the charge to permit characterization of gravitational effects. Fo and diopside (Di) were analyzed for major element concentrations by electron microprobe (JEOL JXA 8200) at UCLA. Acceleration voltage was set to 15 kV, beam current to 15 nA, peak and background counting times were 10 and 5 s. Carbonates and quenched carbonate melts were analyzed with a defocused beam (10 µm diameter) and a current of 10 nA. Peak and background counting times for carbonate analyses were 20 and 10 s. Major element compositions were obtained by averaging 5–100 analyses of mostly large areas of quenched liquids.

Results

Melting relationships in the forsterite–carbonate system

Melting was identified by textural inspection of the polished experimental charges under the scanning electron microscope. Melting takes place mostly at the expense of magnesian calcite (Mg-calcite), and results in diffuse carbonate melt infiltration throughout the Fo matrix (Fig. 1b) or in local melt accumulation in the upper part of the capsule (Fig. 1c). The onset of melting at nominally dry conditions is at 1.0 GPa between 1225 and 1250 °C and at 1.5 GPa between 1275 and 1300 °C. The solidus temperature decreases at 1.0 and 1.5 GPa with increasing bulk H_2O to 3.5 wt% H_2O (Fig. 2): 1 wt% H_2O yields a solidus at 1125–1150 °C, 2 wt% H_2O at 1075–1100 °C and 3.5 wt% H_2O at 1025–1050 °C. Within the investigated temperature range, the solidus temperature then remains between 1025 and 1050 °C with higher bulk H_2O to up to 5 wt% and likely to the maximum investigated water content of 8 wt% H_2O as suggested by the subsolidus experiment CO-108 at 1025 °C, 1.0 GPa (Fig. 2).

Nominally anhydrous melts coexist only with euhedral Fo (Fig. 1b, c), whereas hydrous carbonate melts near the solidus coexist with Fo + Di + Mg-calcite. In hydrous systems, rising temperature leads to successive loss of Mg-calcite and Di (Fig. 2). The Mg-calcite-out boundary is ~ 25 °C higher than the solidus, independent of bulk H_2O. At temperatures greater than Mg-calcite-out, hydrous melt coexists with Fo + Di (Fig. 1d). In the hydrous melting system to about 5–6 wt% bulk H_2O the Di-out locates between 1150–1175 °C, while Di is absent irrespective of temperature at bulk H_2O contents > 6 wt% (Fig. 2).

Quench textures of nominally anhydrous and hydrous carbonate melts are characterized by a heterogeneous dendritic intergrowth of Ca–Mg carbonate and Mg-rich silicate domains. The latter possess a honeycomb structure (Fig. 1e, f) and are compositionally similar to Di. Carbonate melt of run CO-7-1 also quenched to the characteristic dendritic intergrowth texture, but in addition formed patches of carbonate glass near the capsule wall (Fig. 1f). Larger void space or abundant large fluid bubbles (typically 50–300 µm) heterogeneously distributed in the experimental

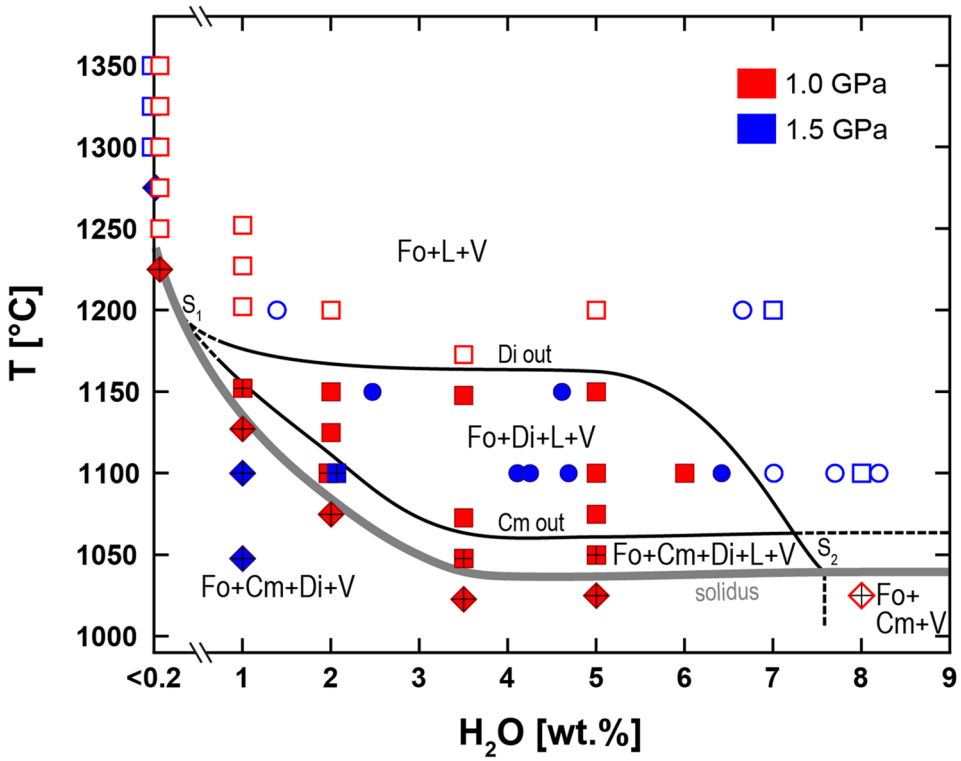

Fig. 2 Temperature vs. bulk H_2O plot showing sub- and super-solidus experiments at 1.0 and 1.5 GPa for unbuffered and buffered runs. All runs are fluid saturated. The solidus temperature is essentially a function of fluid-composition with increasing bulk H_2O-contents leading to an increasing X_{H_2O} in the fluid and an increasing solidus depression until the fluids are H_2O-dominated. Symbol type: circles, unbuffered runs; diamonds, buffered subsolidus runs; squares, buffered runs showing presence of melt phase. Symbols with a black cross have stable magnesian calcite, open symbols lack diopside. The melting curve and the Mg-calcite-out phase boundary decrease in temperature with increasing X_{H_2O} of the coexisting COH-fluid. The liquid composition changes from siliceous Ca-rich carbonatite at the solidus to Mg-rich silico-carbonatite on the expense of Di at temperatures > 1175 °C. Diopside crystallization is restricted to either subsolidus recrystallization of the Fo + Cc starting mix or to the hydrous melting regime. S1 and S2 indicate change in melting reaction (e.g. from eutectic to peritectic or vice versa). Red color for 1.0 GPa, blue color for 1.5 GPa, *Fo* forsterite, *Di* diopside, *Mg-calcite* magnesian calcite, *L* melt, *V* fluid phase

charge indicate fluid saturation during all melting experiments (Fig. 1c). These large bubbles are clearly distinct from tiny micron-sized homogeneous bubbles or voids mostly in between quench crystals, which are ascribed to fluid-exsolution during quench. Fluid saturation was further evidenced by inflated capsules after experiment termination. Globular calcite crystals occur in a majority of hydrous melting experiments (Fig. 1g). These are progressively resorbed by the coexisting carbonate melt as temperature or run duration (> 22–25 h) increase (Supplementary Material S1).

Presence of calcite globules in hydrous melting experiments

The presence of calcite globules in high *P–T* experiments (Wyllie and Tuttle 1960; Maaløe and Wyllie 1975; Kjarsgaard and Hamilton 1988, 1989; Brooker and Hamilton 1990; Kjarsgaard 1998) has led to some debate whether these represent immiscible liquids or crystals. Kjarsgaard and Hamilton (1988, 1989) and Brooker and Hamilton (1990) initially interpreted carbonate spheres in low alkali systems as quenched immiscible liquids that coexisted with CO_2-bearing silicate melt. This interpretation has been revised by the same authors, recognizing that the supposed melt droplets were instead rounded calcite crystals, true carbonate melt droplets always showing some quench texture and a more complex composition (MacDonald et al. 1993; Lee and Wyllie 1996; Brooker and Kjarsgaard 2011, Martin et al. 2013).

Most of our hydrous melting experiments contain up to 50-µm-large calcite globules with sharp contacts to adjacent carbonate melt (Fig. 1g). Similar to subsolidus Mg-calcite the calcite globules are magnesian with 0.98 X_{Ca} and < 0.37 wt% SiO_2. To check whether globular carbonates are metastable or represent an equilibrium phase we have performed a time series across a temperature range from 1050 to 1250 °C, 1.0 GPa (Supplementary Materials S1). Calcite

Table 2 Nominally anhydrous experiments using a H_2-trap double capsule

Run	Mix	*P* (GPa)	*T* (°C)	Time (min)	Phases present	Number analyses	Melt composition (wt%)					
							SiO_2	MgO	CaO	Total	[a]X_{Ca}	[b]CO_2
CO28	A1	1	1225	1440	Fo, Cm, Di, V*	–	–	–	–	–	–	–
CO78	A4	1	1250	465	Fo, L, V	41	7.3 (6)	8.6 (9)	39.6 (8)	55.5	0.77	44.5
CO73	A4	1	1275	315	Fo, L, V	40	7.6 (6)	8.6 (7)	48.4 (6)	64.6	0.8	35.4
CO72	A4	1	1300	200	Fo, L, V	65	7.8 (4)	7.8 (4)	50.1 (4)	65.7	0.82	34.3
CO77	A4	1	1325	310	Fo, L, V	44	7.8 (4)	9.3 (6)	48.5 (5)	65.6	0.79	34.4
CO76	A4	1	1350	305	Fo, L, V	64	7.7 (4)	9.9 (5)	32.4 (5)	50	0.7	50
CO67	A4	1.5	1275	306	Fo, Cm, Di, V*	–	–	–	–	–	–	–
CO64	A4	1.5	1300	595	Fo, L, V	100	8.9 (4)	9.6 (4)	46.8 (3)	65.3	0.78	34.7
CO63	A4	1.5	1300	340	Fo, L, V	100	8.9 (5)	9.6 (5)	46.8 (4)	65.3	0.78	34.7
CO51	A4	1.5	1300	2820	Fo, L, V	30	8.7 (1)	9.4 (1)	43.0 (1)	61.1	0.77	38.9
CO74	A4	1.5	1325	305	Fo, L, V	37	8.8 (6)	8.9 (5)	48.1 (4)	65.8	0.8	34.2
CO75	A4	1.5	1350	350	Fo, L, V	70	8.4 (2)	9.9 (3)	40.2 (2)	58.5	0.75	41.5

Numbers in parentheses denote one standard error (right hand side digit of value)

Fo forsterite, *Cm* magnesian calcite, *Di* diopside, *L* carbonate melt, *V* fluid, *V** fluid saturation indirectly deduced from presence of void space

[a]X_{Ca} represents the molar ratio of CaO/(CaO + MgO)

[b]CO_2 calculated by total difference to 100

globule counts across polished 2-D sections decrease with run duration from 300 to 2900 min or with increasing temperature at constant bulk H_2O content. In 300- to 325-min-long runs between 10 and 157 calcite globules were counted (over approximately 15 mm^2 polished capsule surface), while experiments exceeding 1100 min yielded < 16 Mg-calcite globules. Longer run-times and higher experimental temperatures hence help in resorbing what we interpret to be metastable globular calcite at temperatures higher than the Mg-calcite-out phase boundary. We concur with Lee and Wyllie (1996) that the round habit of calcite is presumably caused by surface tension between the carbonate crystal and the carbonate liquid.

Subsolidus phase assemblage

The subsolidus mineral assemblage consists of Fo, Mg-calcite and Di. Mg-calcite forms up to 75 µm large homogeneous patches free of silicate inclusions within a polygonal Fo + Di crystal matrix (Fig. 1h). Well-developed crystal shapes and chemical homogeneity of the stable mineral phase assemblage suggest attainment of equilibrium after 300 min. Very thin (< 5 µm) films of carbonate-rich quench material coexisting with small (< 10 µm) anhedral Fo and Di crystals (Fig. 1i) occur along Fo–Mg-calcite–Di grain boundaries at nominally anhydrous conditions as well as along the inner surface of nearly spherical fluid voids within the Fo-matrix when bulk H_2O was added. The carbonate-rich quench films are too thin to obtain quantitative electron-microprobe analyses.

Major element composition of carbonate, clinopyroxene and olivine

Calcite is magnesian with an average X_{Ca} of 0.95, its composition does not show significant dependence on bulk water contents or temperature. All clinopyroxenes are diopsidic in composition with 1.95–2.01 Si a.p.f.u. and Ca/Mg ranging from 0.82 to 1.04. Olivine contains up to 0.02 p.f.u. Ca (0.77 wt% CaO) with Si and Mg ranges of 0.96–1.01 and 1.72–2.004 a.p.f.u., respectively with 2.56 a.p.f.u. Fe. Experiments using natural San Carlos olivine yield olivine with 0.86–0.99 X_{Mg}. Mineral compositions are listed in the Supplementary Materials S1.

Melting temperature and melt compositions from experiments with or without the H-trap technique

The effect of H_2O on the melting temperature, melt composition and phase relationships in CaO–MgO–SiO_2–CO_2–H_2O was investigated by two sets of experiments. The first were H-buffered experiments with 60 wt% carbonate primarily aimed at determining near-solidus carbonate melt compositions at nominally anhydrous and controlled hydrous conditions. In practice, large melt fractions diminish the effect of a given amount of H_2O (formed from in-diffusing hydrogen via redox reaction 1). The larger the melt fraction, the lower the H_2O concentration in the melt for a given amount of H_2O, consequently the effect on melting temperature and composition is also reduced. The second type of experiment was unbuffered with respect to hydrogen. These runs used

10 or 20 wt% carbonate to investigate the temperature and pressure dependence of melt compositions in the experiments that allow for H infiltration.

All experiments were fluid saturated. The solidus temperature itself is hence a result of a changing fluid-composition with increasing bulk H_2O content. At dry conditions, the fluid is almost pure CO_2 and does not depress the solidus temperature. With increasing bulk H_2O, the X_{CO_2} in the fluid rapidly decreases and the more H_2O rich the fluid, the larger the solidus depression. At around 3.5 wt% bulk H_2O this effect levels out within the experimental resolution, indicating that the fluid became H_2O-dominated, at which point there is little effect on the solidus temperature.

Buffered melt compositions in large carbonate fraction experiments

At 1250–1350 °C, 1.0 GPa, the nominally anhydrous carbonate melts vary little in SiO_2 from 7.3 to 7.8 wt% (Fig. 3, Table 2). X_{Ca} of the carbonate melts increases from 0.77 at 1250 °C to 0.82 at 1300 °C before a higher dissolution of Si and Mg decreases melt X_{Ca} to 0.70 at 1350 °C (Fig. 4). At 1.5 GPa carbonate melts yield 8.4–8.8 wt% SiO_2 and 0.75–0.80 X_{Ca} (Fig. 4, Table 2).

In contrast, silica contents of hydrous carbonate melts either increase with temperature at a given bulk H_2O content or increase with the amount of fluid added to the experimental charge (Fig. 3) at constant temperature and pressure. For example, at 1.0 GPa and 1 wt% bulk H_2O, melt SiO_2 increases from 6.3 wt% at 1150 °C to 11.4 wt% at 1250 °C (Fig. 3, Table 3). Adding 2 wt% bulk H_2O results in silica melt contents that increase from 7.3 wt% SiO_2 at 1100 °C to 11.1 wt% at 1200 °C. 5 wt% bulk H_2O yields carbonate melts with 10.5 wt% SiO_2 at 1050 °C and 16.1 wt% SiO_2 at 1200 °C (Fig. 3). The X_{Ca} ratios of melts at 1–5 wt% bulk H_2O and 1.0 GPa range from 0.80 to 0.66 and generally decrease with temperature or X_{H_2O} in the coexisting fluid (Fig. 4). At 1100 °C and 2 wt% bulk H_2O, carbonate melt dissolves 7.5 wt% SiO_2 regardless of pressure (Fig. 5). A general pressure sensitivity in the molar Ca:Mg ratio is demonstrated by experiments at 1100 °C and 2 wt% bulk H_2O, where X_{Ca} decreases from 0.73 at 1.0 GPa to 0.66 at 1.5 GPa (Fig. 4, Table 3).

Melt compositions in low carbonate fraction experiments

Buffered melting experiments with $Fo_{0.9}Cc_{0.1}$ yield at 1100 °C and 6 wt% bulk H_2O a carbonate melt with 15.1 wt% SiO_2 and 0.89 X_{Ca} at 1.0 GPa, whereas the addition of 8 wt% H_2O results in a melt with 22.9 wt% SiO_2 and 0.35 X_{Ca} at 1.5 GPa (Figs. 4, 5; Table 3). Melt SiO_2 contents from nominally anhydrous but unbuffered experiments (without using the H-trap) range from 10.6 to 16.1 wt% at 1100 °C to 24.4 wt% at 1200 °C with X_{Ca} ratios between 0.41 and 0.77 at 1.5 GPa (Figs. 4, 5; Table 4). Carbonate melts resulting from unbuffered experiments using the Fe-bearing starting materials B1 and B2 (Table 1) and 2–5 wt% bulk H_2O have 11–26 wt% SiO_2 and 0.48–0.61 X_{Ca} at 1100 °C, 1.5 GPa (Figs. 4, 5; Table 4).

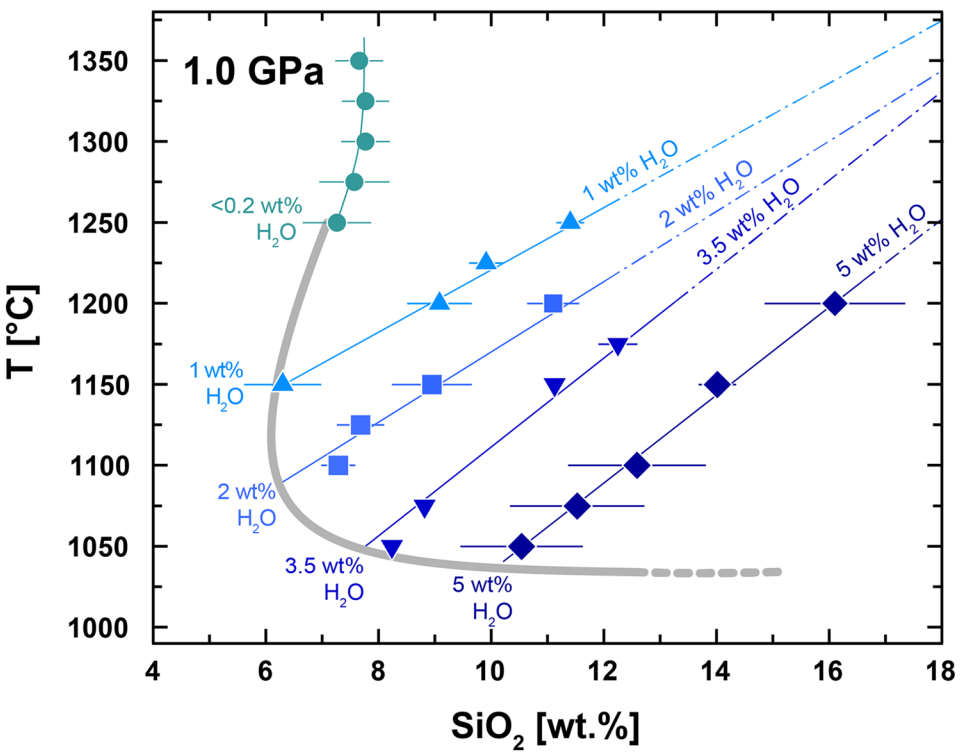

Fig. 3 Temperature vs. melt SiO_2 for 1.0 GPa buffered melt compositions containing 1–5 wt% bulk H_2O contents using the H_2-trap double-capsule technique. Nominally anhydrous melts have 7–8 wt% SiO_2 from 1250–1350 °C, while silica contents of hydrous carbonate melts are strongly sensitive to increasing temperature or to the bulk H_2O contents. Gray solid curve indicates the near-solidus melt SiO_2 evolution as a function of increasing bulk H_2O content

Table 3 Buffered hydrous experiments using a H_2-trap

Run	Mix	H_2O	*P* (GPa)	*T* (°C)	Time (min)	Phases present	Number analyses	Melt composition (wt%)					
								SiO_2	MgO	CaO	Total	$^aX_{Ca}$	$^bCO_2$
CO112	A4	1	1	1125	310	Fo, Cm, Di, V*	–	–	–	–	–	–	–
CO93	A4	1	1	1150	335	Fo, Cm, Di, L, V*	17	6.3 (7)	8.2 (10)	46.5 (10)	61	0.8	39
CO86	A4	1	1	1200	320	Fo, L, V	25	9.1 (6)	8.9 (10)	45.9 (10)	63.9	0.79	36.1
CO88	A4	1	1	1225	315	Fo, L, V	92	9.9 (3)	8.9 (6)	43.8 (3)	62.6	0.78	37.4
CO87	A4	1	1	1250	300	Fo, L, V	81	11.4 (2)	13.3 (5)	41.7 (4)	66.4	0.69	33.6
CO84	A4	2	1	1075	310	Fo, Cm, Di, V*	–	–	–	–	–	–	–
CO80	A4	2	1	1100	325	Fo, Cm, Di, L, V	35	7.3 (3)	11.1 (5)	41.4 (4)	59.8	0.73	40.2
CO83	A4	2	1	1125	300	Fo, Di, L, V	49	7.7 (4)	10.5 (5)	46.8 (5)	65	0.76	35
CO85	A4	2	1	1150	315	Fo, Di, L, V	48	8.9 (7)	10.7 (7)	45.9 (7)	65.5	0.75	34.5
CO81	A4	2	1	1200	300	Fo, L, V	64	11.1 (5)	11.1 (7)	45.5 (6)	67.7	0.75	32.3
CO111	A4	3.5	1	1025	350	Fo, Cm, Di, V*	–	–	–	–	–	–	–
CO104	A4	3.5	1	1050	1190	Fo, Cm, Di, L, V	27	8.2 (5)	12.0 (8)	42.9 (6)	63.1	0.72	36.9
CO110	A4	3.5	1	1075	1380	Fo, Di, L, V	38	8.8 (4)	13.8 (6)	43.5 (5)	66.1	0.69	33.9
CO109	A4	3.5	1	1150	1670	Fo, Di, L, V	30	11.1 (4)	10.0 (7)	46.3 (6)	67.4	0.77	32.6
CO103	A4	3.5	1	1175	1380	Fo, L, V	28	12.2 (3)	10.5 (8)	43.2 (7)	65.9	0.75	34.1
CO94	A4	5	1	1025	335	Fo, Cm, Di, V*	–	–	–	–	–	–	–
CO91	A4	5	1	1050	300	Fo, Cm, Di, L, V	28	10.5 (11)	10.3 (11)	45.1 (9)	65.9	0.76	34.1
CO102	A4	5	1	1075	1540	Fo, Di, L, V	25	11.5 (12)	13.8 (6)	37.8 (7)	63.1	0.66	36.9
CO90	A4	5	1	1100	300	Fo, Di, L, V	28	12.6 (12)	13.1 (7)	42.4 (7)	68.1	0.7	31.9
CO101	A4	5	1	1150	2900	Fo, Di, L, V	36	14.0 (3)	12.8 (5)	40.2 (4)	67	0.69	33
CO95	A4	5	1	1200	305	Fo, L, V	53	16.1 (12)	12.7 (7)	41.8 (7)	70.6	0.7	29.4
CO107	A4	6	1	1100	2700	Fo, Di, L, V	19	15.1 (15)	3.9 (15)	46.9 (12)	65.9	0.9	34.1
CO108	A4	8	1	1025	1395	Fo, Cm, V	–	–	–	–	–	–	–
CO56	A3	1	1.5	1050	1320	Fo, Cm, Di, V*	–	–	–	–	–	–	–
CO60	A1	1	1.5	1100	1395	Fo, Cm, Di, V*	–	–	–	–	–	–	–
CO82	A4	2	1.5	1100	320	Fo, Cm, Di, L, V	6	7.5 (16)	13.6 (23)	37.2 (19)	58.3	0.66	41.7
CO106	A4	7	1.5	1200	1320	Fo, L, V	7	27.8 (23)	18.4 (42)	31.3 (31)	77.5	0.55	22.5
CO100[c]	B3	8	1.5	1100	1765	Fo, L, V	5	22.9 (25)	28.2 (25)	20.8 (31)	81	0.35	19.0

Numbers in parentheses denote one standard error (right hand side digit of value)

Fo forsterite, *Cm* magnesian calcite, *Di* diopside, *L* carbonate melt, *V* fluid, *V** fluid saturation indirectly deduced from presence of void space

[a]X_{Ca} represents the molar ratio of CaO/(CaO + MgO)

[b]CO_2 calculated by total difference to 100

[c]Fe-bearing experiment with melt containing 9.1 (14) wt% FeO

Table 4 Unbuffered nominally anhydrous and hydrous experiments without using a H_2-trap at 1.5 GPa

Run	Mix	[a]H_2O	T (°C)	Time (min)	Phases present	Number analyses	Melt composition (wt%)						
							SiO_2	MgO	CaO	FeO	Total	[b]X_{Ca}	[c]CO_2
[d]CO3-1	B1	7.7	1100	5535	Fo, L, V	16	21.0 (9)	18.3 (9)	23.6 (5)	0.5 (1)	63.4	0.48	36.6
[d]CO6-2	B2	4.2	1100	2820	Fo, L, V	22	10.9 (1)	16.5 (2)	36.4 (2)	1.1 (1)	64.9	0.61	35.1
[e]CO7-1	B2	7.0	1100	3060	Fo, L, V	38	17.9 (1)	18.9 (1)	25.7 (1)	1.0 (1)	63.5	0.49	36.5
[e]CO3-2	B1	8.2	1100	5535	Fo, L, V	40	26.5 (2)	17.3 (3)	23.3 (5)	0.7 (2)	67.8	0.49	32.2
CO2	B1	4.7	1100	2880	Fo, Di, L, V	20	11.8 (3)	19.7 (3)	34.5 (3)	2.8 (6)	68.8	0.56	31.2
CO8-1	A2	4.1	1100	4650	Fo, Di, L, V	20	10.6 (2)	14.2 (5)	38.7 (3)	–	63.5	0.66	36.5
CO7-2	B1	6.4	1100	3060	Fo, Di, L, V	30	16.5 (2)	18.6 (3)	27.3 (2)	0.8 (1)	63.2	0.51	36.8
CO9-1	A2	4.6	1150	2625	Fo, Di, L, V	25	13.3 (2)	19.0 (3)	30.8 (3)	–	63.1	0.54	36.9
CO9-2	A3	2.5	1150	2625	Fo, Di, L, V	26	9.5 (3)	10.3 (3)	32.6 (3)	–	52.4	0.69	47.6
CO10-1	A2	1.4	1200	1350	Fo, Di, L, V	20	9.2 (5)	7.9 (3)	36.3 (4)	–	53.4	0.77	46.6
CO10-2	A3	6.7	1200	1350	Fo, L, V	31	24.4 (1)	23.3 (3)	22.4 (1)	–	70.1	0.41	29.9

Numbers in parentheses denote one standard error (right hand side digit of value)

Fo forsterite, *Di* diopside, *L* carbonate melt, *V* = fluid

[a]Calculated H_2O content by fitting melt SiO_2 of buffered hydrous experiments

[b]X_{Ca} represents the molar ratio of CaO/(CaO + MgO)

[c]CO_2 calculated by total difference to 100

[d]Initially added H_2O content to unbuffered charge = 2 wt% H_2O

[e]Initially added H_2O content to unbuffered charge = 5 wt% H_2O

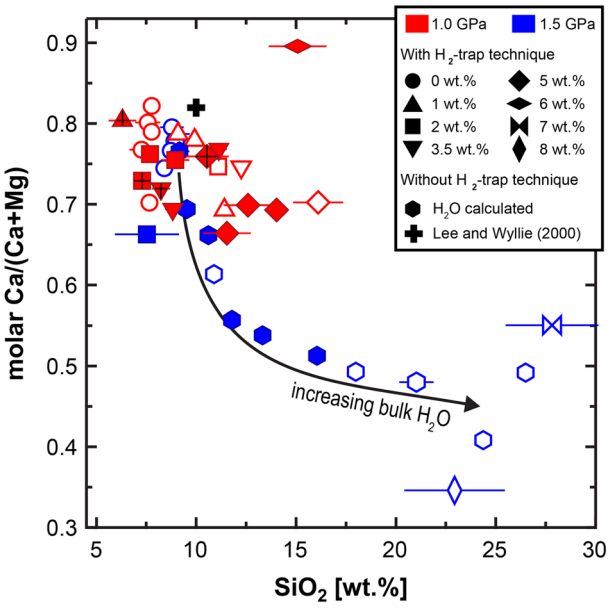

Fig. 4 Molar Ca/(Ca + Mg) plotted against melt SiO_2 at 1.0 and 1.5 GPa represented by red and blue colored symbols, respectively. With decreasing pressure from 1.5 to 1.0 GPa hydrous carbonatites become more Ca-rich. The Mg and Si solubilities in the carbonatite melt increase with X_{H_2O} in the coexisting COH-fluid and result in Mg-rich silico-carbonatites with up to 28 wt% SiO_2 at 1.5 GPa. Symbols with a black cross have stable magnesian calcite, open symbols lack diopside

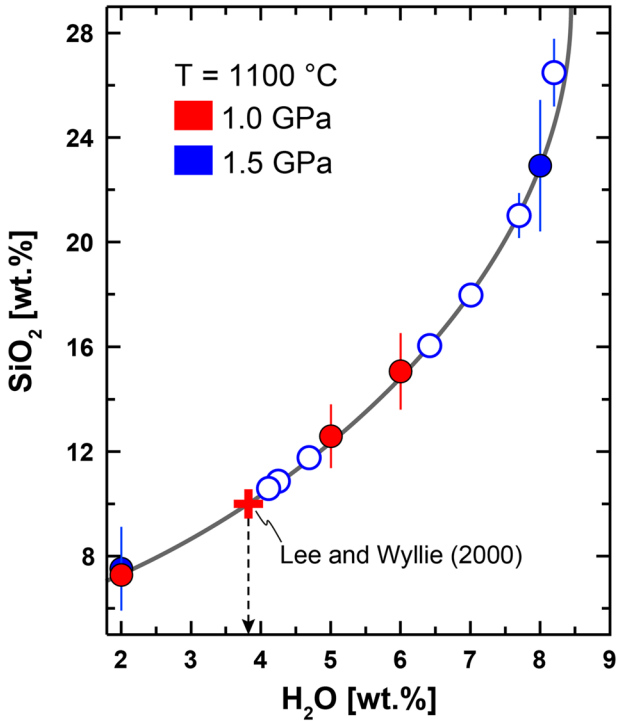

Fig. 5 Melt SiO_2 of buffered and unbuffered melt compositions at 1100 °C plotted against bulk H_2O. SiO_2 in the carbonate melt increases with bulk H_2O; however, keeping the bulk H_2O constant (e.g. 2 wt% H_2O) shows that pressure has a neglectable effect on the silica solubility in carbonate melts between 1.0 and 1.5 GPa. For comparison the nominally anhydrous melt composition (red cross) from Lee and Wyllie (2000) is plotted, who did not account for H infiltration during high-temperature experiments. The melt composition at 1100 °C from Lee and Wyllie (2000) suggests the presence of 3.8 wt% H_2O. Filled circle symbols are double-capsule experiments with known quantities of added H_2O, open circle symbols represent unbuffered experiments. Bulk H_2O contents of unbuffered experiments were calculated from fitted curve of buffered melt compositions (gray curve)

Melt compositions projected from fluid

Melt compositions are projected from fluid into the ternary diagram SiO_2–CaO–MgO (Fig. 6), as justified by saturation in coexisting fluid. At 1250 and 1275 °C, 1.0 GPa, the anhydrous carbonate liquids plot above the Fo–Cc join and at ≥ 1300 °C lie on the Fo–Cc join (gray dashed line in Fig. 6). At 1.5 GPa, the anhydrous carbonate melt plots on the Fo–Cc join at 1350 °C.

At low bulk H_2O (< 2 wt%), carbonate melts lie above the Fo–Cc join. With increasing bulk H_2O, the melts dissolve more MgO and SiO_2 and intersect the Fo–Cc join twice, at ~ 2 and 5 wt% bulk H_2O (Fig. 6). Melt compositions from experiments without the H-trap (systems A2, A3 and B1, B2 in Table 1) plot near the Fo–Cc join at varying CaO:MgO ratios with the exception of four samples that yield significantly higher melt SiO_2 contents at a given molar CaO:MgO ratio (Fig. 6).

Discussion

H_2 gain through noble metals hampers dry solidus determinations

The ability of hydrogen to diffuse through noble metals at elevated temperatures is widely recognized (Knapton 1977; Chou 1986; Truckenbrodt and Johannes 1999; Freda et al. 2001; Hall et al. 2004; Gade et al. 2010) and has been used to control oxygen fugacity (fO_2) in redox-sensitive systems (Eugster 1957; Luth 1989). At temperatures ≥ 1100 °C H infiltration into COH-bearing experimental charges reduces CO_2 or CO_3^{2-} to graphite forming H_2O (Brooker et al. 1998, and references therein). Optical examination under a binocular confirms the blackening of unbuffered run products suggesting the presence of graphite. H-diffusion is effectively diminished by utilizing less permeable sample containers

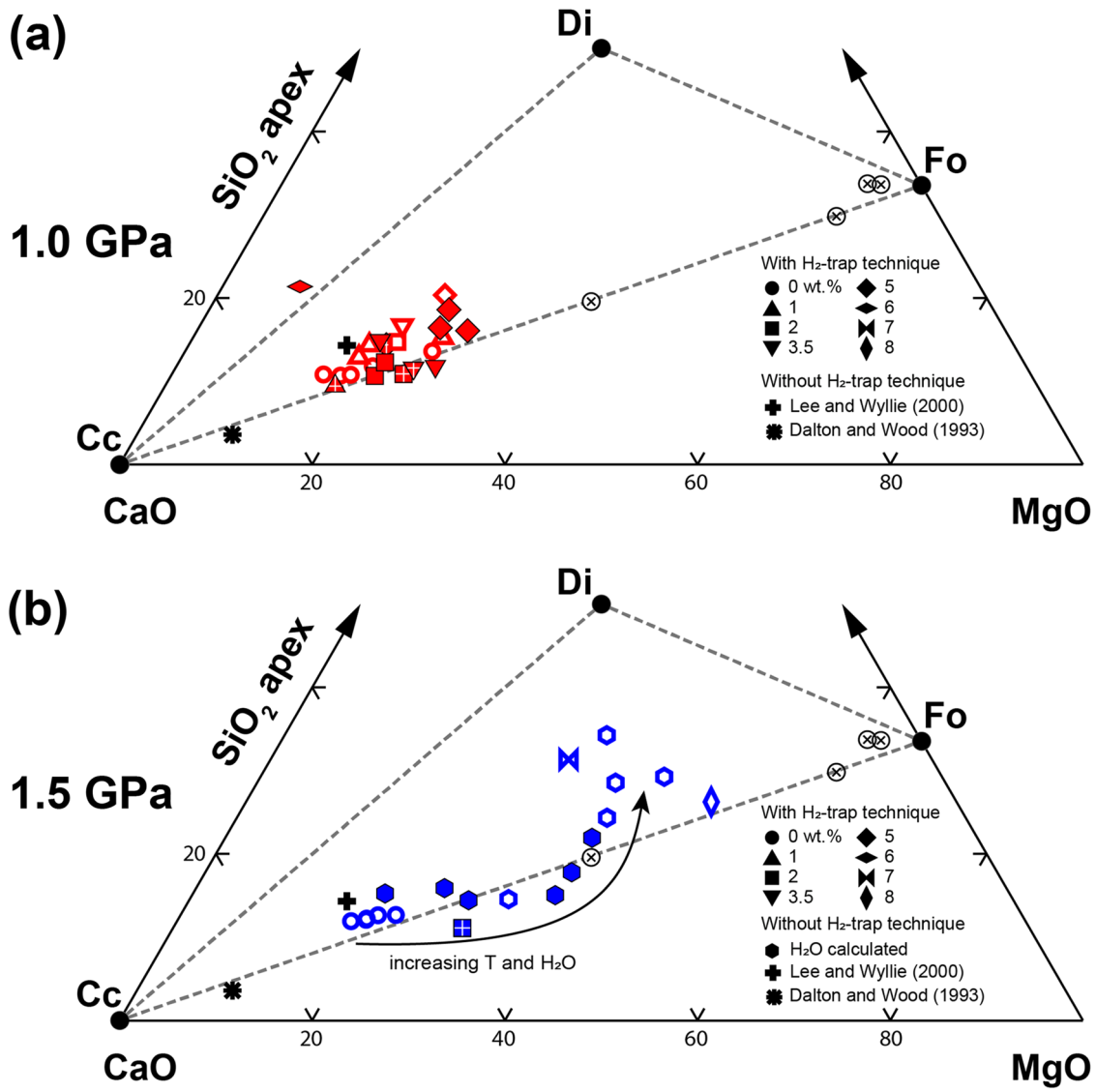

Fig. 6 Anhydrous and hydrous carbonate melt compositions (molar) projected from fluid into the ternary SiO_2–CaO–MgO diagram. The dashed gray lines represent the joins Fo–Cc, Di–Cc and Fo–Di. The arrow depicts an averaged melt evolution with temperature. Open crossed circle locates the $Fo_{40}Cc_{60}$, $Fo_{80}Cc_{20}$ and the $Fo_{90}Cc_{10}$ starting compositions. Nominally anhydrous and hydrous melt compositions from Lee and Wyllie (2000) and Dalton and Wood (1993) are plotted for reference. Crossed-circle symbols represent bulk compositions of experimental starting materials used in this study. The crossing of the diopside-forsterite tie-line results in melting equations changing from eutectic to peritectic

such as AuPd instead of Pt (Knapton 1977; Gade et al. 2010). Kiseeva et al. (2012) compared graphite-lined Pt with AuPd capsules for the melting of carbonated eclogite and reported a difference in solidi of ~ 100 °C. This solidus reduction was attributed to the formation of H_2O upon H_2 gain. However, although Au is less permeable to hydrogen than AuPd or Pt, it cannot entirely prevent H-diffusion at high temperatures (Laporte et al. 2004). Jakobsson (2012) reported a time-dependent increase in bulk H_2O of 25%, from 3.17 to 3.98 wt% H_2O, after 71.6 h at 1200 °C and 1.0 GPa using a Pt–AuPd double-capsule assembly.

We experimentally determined the anhydrous and hydrous solidi using the H-trap double-capsule technique (see section "Experimental Methods"). At 1.0 and 1.5 GPa, the temperatures of the dry solidus are between 1225 and 1250 °C and 1275 and1300 °C, respectively. The experimentally bracketed solidus is regarded as reflecting nominally anhydrous conditions, as we cannot entirely preclude small degrees of hydration during pre-experimental sample preparation. Our nominally anhydrous solidus is 140 °C higher than that of Lee and Wyllie (2000) at 1.0 GPa, 40 °C higher at 1.5 GPa. This difference suggests that

previous attempts to identify carbonated peridotite solidi and phase relationships in natural or model COH systems utilizing unbuffered single capsule experimental designs have been compromised by the presence of unwanted quantities of H_2O through H-induced carbonate reduction (Fig. 5).

At anhydrous subsolidus conditions, the Fo–Cc starting mix in low- and high-carbonate weight fraction experiments recrystallizes to calcic Fo + Mg-calcite + Di. Using average compositions of Mg-calcite and forsterite, mass balance yields the following reaction relation:

$$0.40\,Mg_2SiO_4 + 0.60\,CaCO_3 = 0.38\,Mg_{1.99}Ca_{0.01}SiO_4 + 0.60\,Ca_{0.95}Mg_{0.05}CO_3 + 0.02\,CaMgSi_2O_6, \quad (2)$$

(weight units). In Eq. (2), Mg–Ca cation exchange between Fo and Cc explains the formation of calcic Fo and Mg-calcite. Subsolidus recrystallization in the presence of H_2O results in a threefold increase of Di according to

$$0.40\,Mg_2SiO_4 + 0.60\,CaCO_3 + H_2O = 0.32\,Mg_{1.99}Ca_{0.01}SiO_4 + 0.58\,Ca_{0.95}Mg_{0.05}CO_3 + 0.06\,CaMgSi_2O_6 + COH\text{ - fluid}, \quad (3)$$

which likely relates to an overall higher (molar) solubility of MgO than SiO_2 in COH-bearing fluids compared to pure H_2O. Tiraboschi et al. (2018) investigated the dissolution of Fo–enstatite and Fo–magnesite in pure H_2O and in COH-fluids between 1 and 2 GPa and argued that the observed high MgO solubility in COH-fluids relates to the formation of Mg–C complexes in the graphite-saturated fluids. Fo-equilibrated COH-fluids with 0.85 X_{CO_2} dissolve at 1000–1100 °C, 1.0 GPa up to 6.9 mol MgO/kg H_2O but only 4.6 mol SiO_2/kg H_2O (Tiraboschi et al. 2018). This would translate to a fluid with 1.7 wt% MgO allowing in reaction (3) for 6 wt% Di crystallization, in other words, in the presence of carbonates, forsterite dissolves incongruently in COH-fluids leading to the formation of diopside. At 1.0–1.5 GPa and $T > T_{solidus,}$ anhydrous eutectic melting of calcic Fo + Mg-calcite + Di is mass balanced to

$$0.12\,Mg_{1.99}Ca_{0.01}SiO_4 + 0.85\,Ca_{0.95}Mg_{0.05}CO_3 + 0.03\,CaMgSi_2O_6 = 0.97\,L + 0.03\,CO_2, \quad (4)$$

where L is the CO_2-saturated near-solidus carbonatite melt at 1275 °C and 1.0 GPa (CO-73, Table 2). The excess CO_2 results from the dissolution of Si–Mg component within the carbonate liquid. Hydrous carbonate melting below the Mg-calcite-out is mass-balanced to

$$0.18\,Mg_{1.99}Ca_{0.01}SiO_4 + 0.81\,Ca_{0.95}Mg_{0.05}CO_3 + 0.01\,CaMgSi_2O_6 + H_2O = 1.00\,L + COH\text{ - fluid}, \quad (5)$$

where L represents carbonatite melt at 1050 °C (1.0 GPa) where 3.5 wt% bulk H_2O was added to the Fo–Cc starting mix (run CO-104, Table 3). Increasing temperature at 3.5 wt% bulk H_2O to above the Di-out phase boundary, the melting reaction is mass-balanced to

$$0.19\,Mg_{1.99}Ca_{0.01}SiO_4 + 0.78\,Ca_{0.95}Mg_{0.05}CO_3 + 0.03\,CaMgSi_2O_6 + H_2O = 1.00\,L + COH\text{ - fluid}, \quad (6)$$

representing the carbonatite melt (L) at 1175 °C and 1.0 GPa (run CO-103, Table 3). Fluid phase weight fractions were not considered in the above mass balance reactions because of unknown H_2O and COH-fluid solubility in carbonate melts at pressures > 0.1 GPa.

Effect of H infiltration on melt compositions

To investigate the effect of H infiltration on carbonate melt compositions we performed two sets of unbuffered low-carbonate weight-fraction experiments at 1100 °C and 1.5 GPa adding either 2 or 5 wt% bulk H_2O to the anhydrous starting materials (Tables 1, 4). Adding 5 wt% bulk H_2O results after 92 h in a silico-carbonatite melt with 26.5 wt% SiO_2 and 0.49 X_{Ca}. Significantly lower silica contents of 11 and 18 wt% SiO_2 were observed in 48 h-long experiments containing 2 and 5 wt% bulk H_2O, respectively. This is interpreted to reflect an increasing degree of hydration with run duration through progressive CO_2 or CO_3^{2-} reduction, which ultimately controls the Si-solubility of Fo-equilibrated carbonate melts.

Comparison of the melt SiO_2 contents in unbuffered nominally anhydrous experiments with those in buffered experiments suggests that H-diffusion led to the formation of ≥ 1.4 wt% bulk H_2O (Figs. 3, 4, 5). Lee and Wyllie (2000) reported near-solidus anhydrous carbonate melts with ~ 11 wt% SiO_2 at 1100 °C and 1.0 GPa. Our findings suggest that the unbuffered melt composition from Lee and Wyllie (2000) most likely contained ~ 3.8 wt% bulk H_2O (Fig. 5). In contrast, Dalton and Wood (1993) added at least 1.2 wt% H_2O to their starting materials and reported near-solidus carbonate melts with only 2–3 wt% SiO_2 and ~ 0.9 X_{Ca} at 1150 °C and 1.5 GPa. Such low melt SiO_2 contents were not observed in our melting experiments regardless of bulk water contents.

Carbonate melt evolution in the CaO–MgO–SiO_2 ternary projected from fluid

Figure 7 illustrates the observed phase relations of nominally anhydrous and hydrous carbonate melts at 1.0 and 1.5 GPa. At both pressures, nominally anhydrous near-solidus melts have 7.3–8.9 wt% SiO_2 and lie just above the Fo–Cc join (Figs. 6, 7). The resulting eutectic melting reaction within the Di–Fo–Cc phase stability field requires a thermal maximum on the Fo–Cc tie-line. Nominally dry melts become

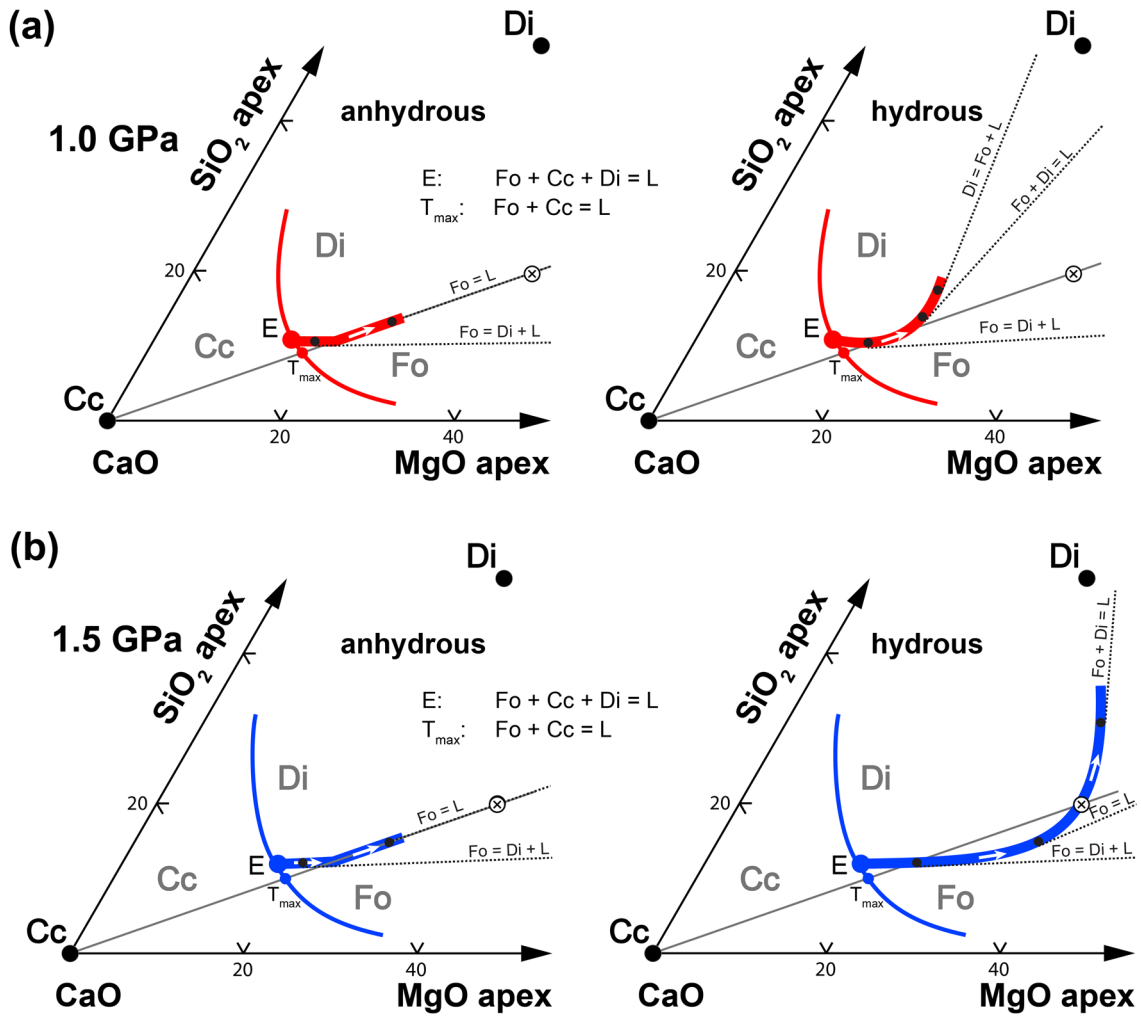

Fig. 7 Schematic sketch illustrating the observed phase relations and melt evolution at 1.0 GPa (top) and 1.5 GPa (bottom) in the ternary SiO_2–CaO–MgO diagram projected from fluid. Gray solid line represents the tie-line between Fo and Cc. Tangents for specific melt evolution steps are drawn as dotted lines and labeled accordingly to the resultant melting reaction at the cotectic. White arrows show the melt evolution path along the cotectic. In nominally anhydrous and hydrous large carbonate fraction experiments the near-solidus melt locates just above the Fo–Cc join resulting in the eutectic melting reaction E, which requires a thermal maximum on the Fo–Cc join. With increasing temperature anhydrous melts become more MgO-rich and intersect the Fo–Cc join at 1300 °C. In presence of COH-fluids, the hydrous cotectic also evolves to Mg concentrations and intersects the join, where the melting reaction changes from eutectic to peritectic (point S1 in Fig. 2). With increasing bulk H_2O contents, hydrous melts yield higher Mg/Ca at relatively constant SiO_2. Further increases in H_2O leads the cotectic to shift to high SiO_2 concentrations while Mg:Ca ratios only change little. The Fo–Cc join is intersected a second time, which causes the melting reaction to change from peritectic to eutectic (point S2 in Fig. 2). Crossed-circle symbols represent the $Fo_{60}Cc_{40}$ bulk composition used in this study

more magnesian with increasing temperature at nearly constant CaO:SiO_2 ratios, leading to an intersection of the cotectic with the Fo–Cc join (Fig. 7).

At low bulk H_2O contents of < 1 wt%, eutectic melting also starts on the silica-rich side of the Fo–Cc join in Fig. 7. With increasing bulk H_2O the resultant carbonate melts dissolve more SiO_2 and MgO along the Fo–Di cotectic and intersects the Fo–Cc join twice, where the melting reaction changes from eutectic to peritectic, and vice versa (points S1 and S2 in Fig. 2). The intersections of the Fo–Di cotectic with the Fo–Cc join are similar to singular points in pressure–temperature space, where Di switches from the reactant- to the product side in melting reaction 3. The Fo–Di cotectic expands with pressure from 1.0 to 1.5 GPa to higher MgO:CaO ratios within the carbonate liquid (Fig. 7), confirming that ascending carbonate mantle melts become more calcic with decreasing pressure (Dalton and Wood 1993).

Absence of a two-liquid field in alkali-free systems

Our hydrous melting experiments at 1.0 and 1.5 GPa yield a continuous compositional spectrum from moderately siliceous carbonate melts to Mg-rich silico-carbonatites (Figs. 3, 4, 5, 6, Tables 3, 4). This demonstrates that in the alkali-free H_2O-rich system, there is no carbonate–silicate melt miscibility gap at 1.0–1.5 GPa. Experimental studies have shown that the size of the two-liquid field primarily depends on pressure, temperature and bulk composition (Freestone and Hamilton 1980; Kjarsgaard and Hamilton 1988; Baker and Wyllie 1990; Kjarsgaard 1990; Brooker 1995). To about 1.5–2 GPa, increasing pressure leads to a slight increase of the miscibility gap (Brooker and Kjarsgaard 2011); however, at higher pressures, the carbonate–silicate melt miscibility gap shrinks and disappears at around 6 GPa (Martin et al. 2013). In alkali-rich eclogites and metapelitic systems, miscibility gaps with clear menisci between the two melts or carbonatite droplets within a silicate melt matrix were described between 3 and 6 GPa (Kiseeva et al. 2012; Thomsen and Schmidt 2008; Tsuno and Dasgupta 2011; Martin et al. 2013; Skora et al. 2015; Mann and Schmidt 2015). In alkali-poor systems, separation between carbonate and silicate melts was also reported at 3–6 GPa for carbonated eclogites (Hammouda 2003; Dasgupta et al. 2006) and at 2–3 GPa for carbonated peridotites (Novella and Keshav 2010; Novella et al. 2014). The two-liquid field reported by Novella and Keshav (2010) and Dasgupta et al. (2006) at 2.4 and 3 GPa were based on observing carbonate-rich quench interstitial within a crystal-rich layer in one capsule portion and pools of silicate melt outside the crystal aggregates in the other capsule portion, neither a contact between the two melts nor any droplets of one melt in the other were observed. Martin et al. (2013) attempted to reproduce these results at identical *P*–*T*–*X* conditions but obtained either single homogeneous CO_2 bearing silicate melts or a single melt and crystals. It was hence concluded that the alleged carbonate liquid of Novella and Keshav (2010) and Dasgupta et al. (2006) resulted from quenching the same CO_2-rich silicate melt as present in the large pools within a silicate crystal matrix. Hence, the silicate melt component forms growth rims on the adjacent silicate crystals leaving behind an interstitial sparry carbonate material. Our experiments corroborate the absence of a miscibility gap in alkali-free and H_2O-rich systems.

In the Na_2O–CaO–MgO–Al_2O_3–SiO_2–CO_2 system, the miscibility gap shrinks with decreasing pressure from 2.5 to 1.0 GPa as well as with decreasing Mg/Ca of the bulk composition (Lee and Wyllie 1992, 1996, 1997). In alkali-rich carbonated nephelinite systems, a miscibility gap at 2.5 GPa results in conjugated liquids rich in Na_2O (Baker and Wyllie 1990). The high sodium concentrations in the silicate and the carbonate melts exceed any realistic mantle melt composition, which led Baker and Wyllie (1990) to conclude that immiscible separation of carbonatites from mantle-derived silicate melts is unlikely to occur at pressures ≥ 2 GPa. In a relatively alkali-poor nephelinite–$CaCO_3$ system, Lee and Wyllie (1997) did not obtain liquid immiscibility at 1.0 GPa, evidencing the role of alkalis in the formation of carbonatites by liquid immiscibility. Brooker and Kjarsgaard (2011) obtained liquid immiscibility in the Na_2O–CaO–Al_2O_3–SiO_2–CO_2 system from 0.1 to 2.5 GPa. They concluded that high CO_2 partial pressure and ≥ 5 wt% $Na_2O + K_2O$ are required within a parental silicate melt prior to unmixing to ensure an intersection of the silicate liquid with the melt miscibility gap at upper mantle pressures.

The silico-carbonatites from this study contain up to 27.8 wt% SiO_2 at relatively low pressures but a miscibility gap does not occur. The absence of a two-liquid field relates to the absence of alkalis and to the presence of high H_2O contents. Small changes in P_{CO_2} greatly affect the size of the miscibility gap, which reaches its maximum extent at CO_2 saturation (Lee and Wyllie 1996; Brooker 1998). Baker and Wyllie (1990) found that the addition of H_2O induces a closure of the miscibility gap, an effect of CO_2 activity reduction (Brooker 1998). According to our results, it is possible to generate a wide range of Si–Mg–Ca–carbonatites in the hydrous upper mantle, giving leeway to the generation of Mg-rich silico-carbonatites at *P*–*T*–*X* conditions relevant to subduction zones (Poli 2015).

Temperature–bulk H_2O window of metasomatic wehrlite formation

Mantle-derived carbonate melts are thought to represent metasomatic agents that transform carbonated lherzolite to wehrlite (Yaxley et al. 1991, 2019,, 1998; Dalton and Wood 1993; Hauri et al. 1993; Rudnick et al. 1993; Coltorti et al. 1999; Lee and Wyllie 2000; Neumann et al. 2002). At pressures > 2 GPa, near-solidus carbonate melts ascending through the upper mantle may reach the "solidus ledge" (characteristic backbend of the CO_2-bearing peridotite solidus within a narrow pressure range), at which carbonatite melts react with orthopyroxene and solidify upon decarbonation to form forsterite + clinopyroxene + CO_2 (Wallace and Green 1988). This prevents rising Ca–Mg–carbonatites from crossing the "solidus ledge" (Wyllie 1980; Schneider and Eggler 1986; Wallace and Green 1988; Dalton and Wood 1993; Dalton and Presnall 1998), unless successive recharge of carbonatites at the carbonated-peridotite solidus depth extends and pushes the "carbonatite-freezing" horizon to lower pressures resulting in the formation of wehrlitic mantle domains (Bailey 1985, 1987). Subsequently generated carbonate melts that equilibrate with Fo and Di can hence ascend through such metasomatized wehrlitic mantle and

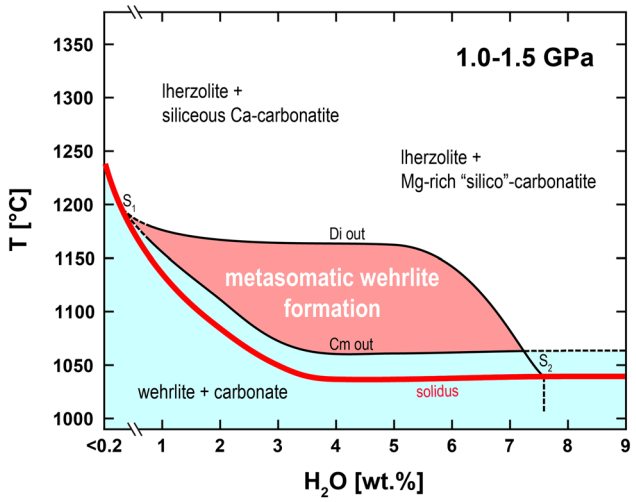

Fig. 8 At subsolidus conditions the stable phase assemblage is Di + Fo + Mg-calcite. Above the solidus, Di is restricted to the hydrous melting regime and disappears at > 1175 °C and > 7 wt% bulk H_2O. At low bulk H_2O contents carbonate melts in equilibrium with Fo are siliceous Ca-rich carbonatites with 7–8 wt% SiO_2, while the Si and Mg solubilities in carbonate melts increase with bulk H_2O leading to the formation of hydrous Mg-rich silico-carbonatites with up to 27.8 wt% SiO_2. Metasomatic transformation from carbonated lherzolite to Mg-calcite-free wehrlite in COH-fluid-saturated systems is restricted to a narrow temperature–X_{H_2O} window at upper mantle pressures of 1.0–1.5 GPa (light red colored field)

eventually may reach shallow crustal levels (Bailey 1985; Dalton and Wood 1993).

Based on our experimental results mantle domains saturated in COH-fluids can metasomatically transform to wehrlite (Figs. 1d, 8). Some of our nominally anhydrous but CO_2-saturated subsolidus experiments yielded 6–10 wt% Di, which exceeds the maximum of 2 wt% Di according to subsolidus mass-balance reaction (2). At pressures between 1.0 and 1.5 GPa, such a threefold increase in Di weight fraction is best explained by a high Mg/Si-solubility in COH-fluids compared to pure H_2O (Tiraboschi et al. 2018), which is coherent with the hydrous mass-balance subsolidus reaction (3). Even in nominally anhydrous experiments using the H-trap double-capsule technique, we cannot entirely exclude trace amounts of H_2O that may either result from the smallest fraction of infiltrating hydrogen during the experiment or, more likely, from moisture during sample preparation. Hence, the presence of Di in our nominally anhydrous subsolidus experiments suggests a minor degree of H_2O contamination.

Traces of H_2O contamination in our nominally anhydrous melting experiments are unlikely to affect the determination of near-solidus melt compositions or phase equilibria because moving the bulk starting mix towards the minimum melt composition results in large amounts of melt at the solidus, which in turn minimizes the effect of H on melting.

At super-solidus temperatures, Di crystallization is restricted to the hydrous melting regime at < 1175 °C and < 7 wt% bulk H_2O (Figs. 2, 8). Rising temperature above the Mg-calcite-out phase boundary at a given bulk H_2O progressively increases the carbonate melt solubility in Si and Mg, which leads to the formation of hydrous silico-carbonatites with up to 27.8 wt% SiO_2 and 18.4 wt% MgO (Figs. 4, 5, 6). Our results thus demonstrate that wehrlite may either form at COH-saturated subsolidus conditions or during carbonate melt interaction with hydrated upper mantle domains (Fig. 8).

Conclusions

In comparison to previous studies, the temperature discrepancy to our nominally anhydrous solidus in $CaO–MgO–SiO_2–CO_2$ is + 140 °C to + 40 °C at 1.0–1.5 GPa, which can be explained by hydration of unbuffered experimental charges through H-diffusion. Previous studies on CO_2 or CO_3^{2-}-bearing anhydrous systems were likely compromised by the unwanted presence of H_2O ranging from trace amounts to the weight percent level. Our data show that melting in $CaO–MgO–SiO_2–CO_2–H_2O$ strongly depends on the X_{H_2O} of the coexisting COH-fluid. In temperature-X_{H_2O} space, hydrous melting sets in ~ 25 °C below the Mg-calcite-out and decreases to temperatures as low as 1025–1050 °C at bulk H_2O contents exceeding 2 wt%. In the presence of COH-fluids, the Mg-calcite-out gives leeway for a progressively increasing Si–Mg dissolution within the carbonate melt as temperature and X_{H_2O} increase, suggesting that Mg-rich silico-carbonatites can be generated in COH-saturated upper mantle at relatively low temperatures of < 1050 °C and pressures equivalent to ~ 35–50 km depth. A two-liquid field is absent in alkali-free systems allowing Si–Mg-rich carbonatites to exist in equilibrium with wehrlitic mantle. Furthermore, our results demonstrate the important role of COH-fluids in metasomatically transforming carbonated lherzolite to wehrlite. Infiltration of slab derived, initially carbonate saturated fluids leads to carbonatite melts when rising fluids reach the appropriate solidus temperature within the mantle wedge. Apparently, such carbonatites are not erupted, they are generally absent in arcs. Most likely, their very low viscosity and favorable wetting properties hinders the channelization of such liquids. If these carbonate melts just pervasively progress upwards along grain boundaries, they will simply precipitate carbonate when topping out of the hot part of the mantle wedge, i.e. when temperature decreases to subsolidus conditions. Consequently, COH-fluids rising from the slab may lead to important chemical changes in the mantle wedge.

Acknowledgements This study was financed by SNF grants P2EZP2_162274 and P300P2_177798 and supported by ETH Grant 34-11-1. Financial support by the Deep Carbon Observatory for experimental consumables is acknowledged. M. De Paoli, M. Galvez and C. Liebske are thanked for a critical appraisal of an earlier version of the manuscript as well as for valuable discussions. A. Makhluf and R. Esposito are thanked for technical support in the high-pressure and EPMA lab at UCLA. R.C. Newton is gratefully acknowledged for technical support in designing the H-trap double-capsule technique and for manufacturing high-precision piston-cylinder assembly parts as well as for many insightful discussions.

References

Bailey DK (1985) Fluids, melts, flowage and styles of eruption in alkaline ultramafic magmatism. Trans Geol Soc S Afr 88:449–457

Bailey DK (1987) Mantle metasomatism—perspective and prospect. In: Fitton JG, Upton BGJ (eds) Alkaline igneous rocks. Geological Society, London, Special Publication, vol 30, pp 1–13

Baker MB, Wyllie PJ (1990) Liquid immiscibility in a nephelinite–carbonate system at 25 kbar and implications for carbonatite origin. Nature 346:168–170

Boyd FR, England JL (1963) Some effects of pressure on phase relations in the system $MgO–Al_2O_3–SiO_2$. Carnegie Inst Wash Yearb 62:121–124

Brey GP, Bulatov VK, Girnis AV (2009) Influence of water and fluorine on melting of carbonated peridotite at 6 and 10 GPa. Lithos 112:249–259

Brooker RA, Hamilton DL (1990) Three-liquid immiscibility and the origin of carbonatites. Nature 346:459

Brooker RA (1995) Carbonatite genesis: an experimental evaluation of the role of liquid immiscibility to 25 kilobars. Ph.D. thesis, University of Manchester

Brooker RA (1998) The effect of CO_2 saturation on immiscibility between silicate and carbonate liquids: an experimental study. J Petrol 39:1905–1915

Brooker R, Holloway JR, Hervig R (1998) Reduction in piston-cylinder experiments: the detection of carbon infiltration into platinum capsules. Am Mineral 83:985–994

Brooker RA, Kjarsgaard BA (2011) Silicate-carbonate liquid immiscibility and phase relations in the system $SiO_2–Na_2O–Al_2O_3–CaO–CO_2$ at 0.1–2.5 GPa with applications to carbonatite genesis. J Petrol 52:1281–1305

Chou IM (1986) Permeability of precious metals to hydrogen at 2-kb total pressure and elevated-temperatures. Am J Sci 286(8):638–658

Chou IM, Eugster HP (1978) Diffusion of hydrogen through platinum membranes at high pressures and temperatures. Geochim Cosmochim Acta 42:281–288

Coltorti M, Bonadiman C, Hinton RW, Siena F, Upton BGJ (1999) Carbonatite metasomatism of the oceanic upper mantle: evidence from clinopyroxenes and glasses in ultramafic xenoliths of Grande Comore, Indian Ocean. J Petrol 40:133–165

Dalton JA, Wood BJ (1993) The compositions of primary carbonate melts and their evolution through wallrock reaction in the mantle. Earth Planet Sci Lett 119:511–525

Dalton JA, Presnall DC (1998) The continuum of primary carbonatitic–kimberlitic melt compositions in equilibrium with lherzolite: data from the system $CaO–MgO–Al_2O_3–SiO_2–CO_2$ at 6 GPa. J Petrol 39:1953–1964

Dasgupta R, Hirschmann MM, Withers AC (2004) Deep global cycling of carbon constrained by the solidus of anhydrous, carbonated eclogite under upper mantle conditions. Earth Planet Sci Lett 227:73–85

Dasgupta R, Hirschmann MM, Stalker K (2006) Immiscible transition from carbonate-rich to silicate-rich melts in the 3 GPa melting interval of eclogite + CO_2 and genesis of silica-undersaturated ocean island lavas. J Petrol 47:647–671

Dasgupta R, Hirschmann MM (2010) The deep carbon cycle and melting in Earth's interior. Earth Planet Sci Lett 298:1–13

Eugster HP (1957) Heterogeneous reactions involving oxidation and reduction at high pressures and temperatures. J Chem Phys 26:1760–1761

Falloon TJ, Green DH (1989) The solidus of carbonated, fertile peridotite. Earth Planet Sci Lett 94:364–370

Freda C, Baker DR, Ottolini L (2001) Reduction of water loss from gold-palladium capsules during piston-cylinder experiments by use of pyrophyllite powder. Am Mineral 86(3):234–237

Freestone IC, Hamilton DL (1980) The role of liquid immiscibility in the genesis of carbonatites—an experimental study. Contrib Mineral Petrol 73:105–117

Gade SK, Coulter KE, Way JD (2010) Effects of fabrication technique upon material properties and permeation characteristics of palladium–gold alloy membranes for hydrogen separations. Gold Bull 43(4):287–297

Hall LJ, Brodie J, Wood BJ, Carroll MR (2004) Iron and water losses from hydrous basalts contained in $Au_{80}Pd_{20}$ capsules at high pressure and temperature. Mineral Mag 68(1):75–81

Hammouda T (2003) High-pressure melting of carbonated eclogite and experimental constraints on carbon recycling and storage in the mantle. Earth Planet Sci Lett 214:357–368

Hauri EH, Shimizu N, Dieu JJ, Hart ST (1993) Evidence for hotspot-related carbonatite metasomatism in the oceanic upper mantle. Nature 365:221–227

Hazen RM, Downs RT, Jones AP, Kah L (2013) Carbon mineralogy and crystal chemistry. Rev Mineral Geochem 75:7–46

Huebner JS (1971) Buffering techniques for hydrostatic systems at elevated pressures. In: Ulmer EC (ed) Research techniques for high pressure and high temperature. Springer, Berlin, pp 123–177

Jakobsson S (2012) Oxygen fugacity control in piston-cylinder experiments. Contrib Mineral Petrol 164:397–406

Keppler H (2003) Water solubility in carbonatite melts. Am Mineral 88:1822–1824

Kiseeva ES, Yaxley GM, Hermann J, Litasov KD, Rosenthal A, Kamenetsky VS (2012) An experimental study of carbonated eclogite at 3.5–5.5 GPa—implications for silicate and carbonate metasomatism in the cratonic mantle. J Petrol 53:727–759

Kjarsgaard BA, Hamilton DL (1988) Liquid immiscibility and the origin of alkali-poor carbonatites. Mineral Mag 52:43–55

Kjarsgaard B, Hamilton DL (1989) Carbonatite origin and diversity. Nature 338:547–548

Kjarsgaard BA (1990) Nephelinite–carbonatite genesis: experiments on liquid immiscibility in alkali silicate–carbonate systems. Ph.D. thesis, University of Manchester, England

Kjarsgaard BA (1998) Phase relations of a carbonated high-CaO nephelinite at 0.2 and 0.5 GPa. J Petrol 39(11–12):2061–2075

Knapton AG (1977) Palladium alloys for hydrogen diffusion membranes. A review of high permeability materials. Platin Met Rev 21(2):45–50

Laporte D, Toplis MJ, Seyler M, Devidal JL (2004) A new experimental technique for extracting liquids from peridotite at very low degrees of melting: application to partial melting of depleted peridotite. Contrib Mineral Petrol 146:463–484

Lee W, Wyllie PJ (1992) Liquid immiscibility between silicates and carbonates must intersect suitable liquidus field boundaries to have petrogenetic significance. In: 29th international geology congress, vol 2, p 571

Lee WJ, Wyllie PJ, Rossman GR (1994) CO_2-rich glass, round calcite crystals, and no liquid immiscibility in the system CaO–SiO_2–CO_2 at 2.5 GPa. Am Mineral 79(11–12):1135–1144

Lee WJ, Wyllie PJ (1996) Liquid immiscibility in the join $NaAlSi_3O_8$–$CaCO_3$ to 2.5 GPa and the origin of calciocarbonatite magmas. J Petrol 37:1125–1152

Lee WJ, Wyllie PJ (1997) Liquid immiscibility between nephelinite and carbonatite from 1.0 to 2.5 GPa compared with mantle melt compositions. Contrib Mineral Petrol 127:1–16

Lee WJ, Wyllie PJ (2000) The system CaO-MgO-SiO_2–CO_2 at 1 GPa, metasomatic wehrlites, and primary carbonatite magmas. Contrib Mineral Petrol 138:214–228

Lee WJ, Huang WL, Wyllie P (2000) Melts in the mantle modeled in the system CaO–MgO–SiO_2–CO_2 at 2.7 GPa. Contrib Mineral Petrol 138:199–213

Luth RW (1989) Natural versus experimental control of oxidation state: effects on the composition and speciation of C–O–H fluids. Am Mineral 74:50–57

Maaløe S, Wyllie PJ (1975) The join grossularite-calcite through the system CaO–Al_2O_3–SiO_2–CO_2 at 30 kilobars: crystallization range of silicates and carbonates on the liquidus. Earth Planet Sci Lett 28(2):205–208

Macdonald R, Kjarsgaard BA, Skilling IP, Davies GR, Hamilton DL, Black S (1993) Liquid immiscibility between trachyte and carbonate in ash flow tuffs from Kenya. Contrib Miner Petrol 114(2):276–287

Mann U, Schmidt MW (2015) Melting of pelitic sediments at subarc depths: 1. Flux vs. fluid-absent melting and a parameterization of melt productivity. Chem Geol 404:150–167

Manning CE (1994) The solubility of quartz in H_2O in the lower crust and upper mantle. Geochim Cosmochim Acta 58:4831–4839

Martin LHJ, Schmidt MW, Mattsson HB, Guenther D (2013) Element partitioning between immiscible carbonatite and silicate melts for dry and H_2O-bearing systems at 1–3 GPa. J Petrol 54:2301–2338

Neumann E-R, Wulff-Pedersen E, Pearson NJ, Spencer EA (2002) Mantle xenoliths from Tenerife (Canary Islands): evidence for reactions between mantle peridotites and silicic carbonatite melts inducing Ca metasomatism. J Petrol 43:825–857

Novella D, Keshav S (2010) Silicate melt-carbonatite liquid immiscibility reconsidered in the system CaO–MgO–Al_2O_3 at 2–3 GPa. In: EMPG XIII, Toulouse, conference abstracts

Novella D, Keshav S, Gudfinnsson GH, Ghosh S (2014) Melting phase relations of model carbonated peridotite from 2 to 3 GPa in the system CaO–MgO–Al_2O_3–SiO_2–CO_2 and further indication of possible unmixing between carbonatite and silicate liquids. J Geophys Res Solid Earth 119:2780–2800

Olafsson M, Eggler DH (1983) Phase relations of amphibole, amphibole–carbonate, and phlogopite–carbonate peridotite: petrologic constraints on the asthenosphere. Earth Planet Sci Lett 64:305–315

Poli S (2015) Carbon mobilized at shallow depths in subduction zones by carbonatitic liquids. Nat Geosci 8:633–636

Rudnick RL, McDonough WF, Chappell BW (1993) Carbonatite metasomatism in the northern Tanzanian mantle: petrographic and geochemical characteristics. Earth Planet Sci Lett 114:463–475

Schneider ME, Eggler DH (1986) Fluids in equilibrium with peridotite minerals: implications for mantle metasomatism. Geochim Cosmochim Acta 50:711–724

Skora S, Blundy JD, Brooker RA, Green EC, de Hoog JC, Connolly JA (2015) Hydrous phase relations and trace element partitioning behaviour in calcareous sediments at subduction-zone conditions. J Petrol 56:953–980

Thomsen TB, Schmidt MW (2008) Melting of carbonated pelites at 2.5–5.0 GPa, silicate–carbonatite liquid immiscibility, and potassium–carbon metasomatism of the mantle. Earth Planet Sci Lett 267:17–31

Tiraboschi C, Tumiati S, Sverjensky D, Pettke T, Ulmer P, Poli S (2018) Experimental determination of magnesia and silica solubilities in graphite-saturated and redox-buffered high-pressure COH fluids in equilibrium with forsterite + enstatite and magnesite + enstatite. Contrib Mineral Petrol 173(1):2

Truckenbrodt J, Johannes W (1999) H_2O loss during piston-cylinder experiments. Am Mineral 84(9):1333–1335

Tsuno K, Dasgupta R (2011) Melting phase relation of nominally anhydrous, carbonated politic–eclogite at 2.5–3.0 GPa and deep cycling of sedimentary carbon. Contrib Mineral Petrol 161:743–763

Tumiati S, Fumagalli P, Tiraboschi C, Poli S (2013) An experimental study on COH-bearing peridotite up to 3.2 GPa and implications for crust–mantle recycling. J Petrol 54:453–479

Wallace ME, Green DH (1988) An experimental determination of primary carbonatite magma composition. Nature 335:343–346

Wendlandt RF, Huebner JS, Harrison WJ (1982) The redox potential of boron nitride and implications for its use as a crucible material in experimental petrology. Am Mineral 67:170–174

Wood BJ, Li J, Shahar A (2013) Carbon in the core: its influence on the properties of core and mantle. Rev Mineral Geochem 75:231–250

Wyllie PJ, Tuttle OF (1960) The system CaO–CO_2–H_2O and the origin of carbonatites. J Petrol 1:1–46

Wyllie PJ, Huang WL (1976) Carbonation and melting reactions in the system CaO–MgO–SiO_2–CO_2 at mantle pressures with geophysical and petrological applications. Contrib Mineral Petrol 54(2):79–107

Wyllie PJ (1980) The origin of kimberlite. J Geophys Res B 85:6902–6910

Yaxley GM, Crawford AJ, Green DH (1991) Evidence for carbonatite metasomatism in spinel peridotite xenoliths from western Victoria, Australia. Earth Planet Sci Lett 107:305–317

Yaxley GM, Green DH, Kamenetsky V (1998) Carbonatite metasomatism in the southeastern Australian lithosphere. J Petrol 39(11–12):1917–1930

Yaxley GM, Brey GP (2004) Phase relations of carbonate-bearing eclogite assemblages from 2.5 to 5.5 GPa: implications for petrogenesis of carbonatites. Contrib Mineral Petrol 146:606–619

Yaxley GM, Ghosh S, Kiseeva E, Mallik A, Spandler C, Thomson A, Walter M (2019) CO_2-rich melts in earth. In: Orcutt B, Daniel I, Dasgupta R (eds) Deep carbon: past to present. Cambridge University Press, Cambridge, pp 129–162